Available online at www.sciencedirect.com
SCIENCE DIRECT®
Journal of the European Ceramic Society 25 (2005) 703–710
www.elsevier.com/locate/jeurceramsoc

High temperature mullite dissolution in ceramic bodies derived from Al-rich sludge

M. J. Ribeiro [a], D. U. Tulyagavov [b], J. M. Ferreira [b], J. A. Labrincha [b,*]

[a] *ESTG, Polytechnique Institute of Viana do Castelo, 4900 Viana do Castelo, Portugal*
[b] *Ceramics and Glass Engineering Department, CICECO, University of Aveiro, 3810-193 Aveiro, Portugal*

Received 6 November 2003; received in revised form 10 March 2004; accepted 21 March 2004

Available online 20 June 2004

Abstract

Mullite-based refractory ceramic materials were produced from an industrial Al-rich sludge derived from wastewater treatment of aluminium anodising or surface coating industrial processes, and other low cost raw materials (ball clay, kaolin and diatomite). Cylindrical samples processed by uniaxial dry pressing (32 MPa) were sintered at various temperatures (1250–1650 °C) to study the mullitisation process. The performance of the materials at high temperature (1650 °C) was evaluated through different techniques (XRD, SEM/EDS, optical microscopy, and impedance spectroscopy) to access the microstructural changes occurring under prolonged tests (dwell times up to 100 h). For dwell times <80 h, a preferential dissolution of the smaller mullite grains in the glassy phase and its partial re-precipitation onto the coarser ones, leading to an overall coarsening of the mullite crystals. For dwell times >80 h, coarse α-alumina and Cr-doped alumina developed at the surface of the specimens, being accompanied by the formation of pores in the vicinity of alumina grains. Near alumina grains, additional relevant features include the increase of surface roughness, the appearance of concentration gradients within the glassy phase, which became almost depleted in Al and enriched in alkalines. The continuity of the glassy phase and its enrichment in alkaline species enhanced the electrical conductivity of the material, enabling the use of impedance spectroscopy to access the microstructural changes occurring during prolonged heat treatment.

Keywords: Sintering; Microstructure-final; Thermal properties; Mullite; Al_2O_3

1. Introduction

In the past few decades, a great deal of research work has been devoted to mullite ceramics as a high temperature engineering material, including different techniques used to obtain this crystalline phase.[1–4] Most of the kinetic studies on mullite formation usually appear associated to the decomposition reactions of kaolinite (the predominant clay mineral in kaolins) on heating, and to the sintering ability of porcelains.[5–12]

Chen et al.[9] have shown that the phase evolution of a kaolin on heating up to 1600 °C was as follows:

1. At $T \approx 400$–$600\,^{\circ}C$: $2SiO_2 \cdot Al_2O_3 \cdot 2H_2O$ (kaolinite) → $2SiO_2 \cdot Al_2O_3$ (metakaolinite) + $2H_2O$;
2. At $T \approx 980\,^{\circ}C$: $2SiO_2 \cdot Al_2O_3$ (metakaolinite) → $SiAl_2O_5$ (spinel) + SiO_2 (amorphous); or $2SiO_2 \cdot Al_2O_3$ (metakaolinite) → Al_2O_3 (γ-alumina) + $2SiO_2$ (amorphous);
3. For $T > 1100\,^{\circ}C$: $SiAl_2O_4$ (spinel) + SiO_2 (amorphous) → $1/3(3Al_2O_3 \cdot 2SiO_2)$ (mullite)+$4/3SiO_2$ (amorphous); or Al_2O_3 (γ-alumina) + $2SiO_2$ (amorphous) → $1/3$ $(3Al_2O_3 \cdot 2SiO_2)$ (mullite) + $4/3SiO_2$ (amorphous);
4. For $T > 1200\,^{\circ}C$: amorphous silica gradually transforms into crystoballite, while for $T > 1500\,^{\circ}C$, crystoballite transforms again into amorphous silica.[9]

Other authors[8,11–14] also refer to the formation of primary mullite, $Al_2O_3 \cdot SiO_2$ (mullite 1:1) at around 1100 °C from the Si–O–Al linkages existing in metakaolinite. As the temperature increases ($T > 1200\,^{\circ}C$) the primary mullite crystals start to grow by reacting with the amorphous aluminosilicate phase forming the so called secondary mullite, $3Al_2O_3 \cdot 2SiO_2$ (mullite 3:2). This phase usually exhibits

* Corresponding author. Tel.: +351-234370250; fax: +351-234425300.
E-mail addresses: jmf@cv.ua.pt (J.M. Ferreira), jal@cv.ua.pt (J.A. Labrincha).

0955-2219/$ – see front matter © 2004 Elsevier Ltd. All rights reserved.
doi:10.1016/j.jeurceramsoc.2004.03.028

acicular shaped crystals that exert a beneficial strengthening effect in the firing porcelain bodies in order to minimise warpage.

Besides primary and secondary mullites, Lee and Iqbal[8,11,12] also identified a third type of more elongated mullite crystals, tertiary mullite, formed within the liquid phase where the composition was richer in alumina. Recently, Olhero et al.[13] used different porcelain formulations, some including kaolin, and one in which this component was replaced by a kaolinitic stoichiometric mixture of silica and alumina, pseudo kaolin. It was showed that instead of the secondary mullite crystals observed in the fired samples containing kaolinite, very fine and long tertiary mullite crystals have been formed in the vicinity of corundum grains.

Baudín and Villar[15] studied the influence of the thermal treatment within the temperature range of 900–1630 °C, on the microstructure of the 3:2 mullite in the presence of low content of alkaline oxides. They concluded that the presence of 0.28 wt.% ($Na_2O + K_2O + CaO$), as main impurities, enables a microstructural development, which comprises three main steps: dissolution of mullite grains; formation of a liquid phase; and the grain growth from the liquid phase. As temperature increases, the grain growth from the liquid phase overlaps the dissolution of mullite grains and a bimodal microstructure develops, with an increasing fraction of large tabular grains.

The starting composition, and especially the alumina/silica ratio, determine the evolution of mulite crystals growth.[13,16] Furthermore, the mullitisation reaction process is accomplished at lower temperatures if the proportion of alumina in the sample is above the stoichiometric composition of mullite. On the other hand, if the alumina content is too high, the excess alumina might undergo structural rearrangements and give rise to the formation of α-alumina. Since in the silica–alumina system mullite is thermodynamically more stable than α-alumina, the growth of α-alumina is not expected to occur at the expense of the mullite already formed.[17,18]

However, the reverse transformation of mullite into α-alumina and glassy phase (GP) that might occur at high temperatures, especially in the presence of alkalis, is poorly described in the literature. In the present work the mullitisation process of an already tested composition[19,20] based on Al-rich sludge and other low cost raw materials was first studied in the temperature range of 1250–1650 °C. Then, the microstructural evolution over prolonged heat treatment at 1650 °C (dwell time up to 100 h) was studied, as an attempt to evaluate the performance of the material under high temperature environments. The microstructural changes included mullite dissolution and re-precipitation, coarsening of microstructure, and the subsequent alumina crystallisation, preferentially at the surface of the specimens. Studies involving recycling of Al-rich sludges might have high economic, social and environmental impacts if one considers that only in EU countries, about 100,000 metric tonnes per year of this sludge are currently generated[21] and that no interesting applications were implemented up to now. Moreover, the general characteristics of this kind of sludge were found to be reasonably constant, irrespective of its origin.[22]

2. Experimental procedure

The formulation used in the present work include an Al-rich sludge as the main component (42 wt.%), 15 wt.% of a plastic ball clay (BM-8, Barracão-Leiria, PT), 15 wt.% of kaolin (Mibal-B, Barqueiros, PT), and 28 wt.% of a pre-calcined (600 °C) diatomite (Sociedade Anglo-Portuguesa de Diatomites, Óbidos, PT). The Al-rich sludge derived from the wastewater treatment unit of an aluminium anodising or surface coating industrial plant (Extrusal S.A., Aveiro, PT) and was used after calcination (1400 °C, 2 h). The full characterisation of the raw materials is given elsewhere.[19,20]

Cylindrical samples ($\phi = 25$ mm, with 3 mm thick) were processed by uniaxial dry pressing at about 32 MPa, and sintered at different temperatures (1250–1650 °C). For the samples fired at 1650 °C, seven different dwell times were used: 1, 10, 20, 40, 60, 80 and 100 h. The crystalline phases developed along the heat treatments were detected by XRD (Rigaku Denk Co.). The microstructural and chemical changes were evaluated by SEM/EDS (Hitachi, S4100) after polishing and etching with a 5 (v/v) HF solution for 2–4 min. Stereological measurements were also conducted (a mesh with 120 lines was made containing 6–15 grains) in order to evaluate the average grain size and the volumetric ratio between mullite, alumina and glassy phases, according to the methodology described elsewhere.[23]

Samples were electroded with porous Pt and their electrical behaviour was studied by impedance spectroscopy. Measurements were conducted between 340 and 1020 °C in a experimental set-up, using an Hewlett Packard 4284A bridge and changing the frequency between 20 and 10^6 Hz. Fitting and interpretation of curves was done by using a specific routine program based on NLLS analysis.[24] The electrical response of sintered bodies was then correlated with microstructural and crystalline phase evolutions in order to evaluate the ability of impedance spectroscopy to predict processing–sintering-related properties.

3. Results and discussion

The evolution of crystalline phases along the mullitisation process in the temperature range from 1250 to 1650 °C can be observed in Fig. 1. At 1250 °C, mullite has already been formed, being one of the main crystalline phases, co-existing with cristoballite, alumina and small amounts of α-quartz. With temperature increasing, the intensity of XRD peaks of mullite increases while those of the other crystalline phases tend to vanish. Accordingly, although all of these crystalline phases are still present at 1350 °C, only a residual amount

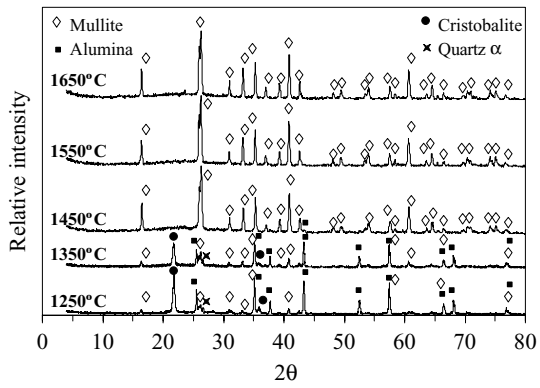

Fig. 1. XRD patterns of powdered samples fired at five different temperatures for 1 h.

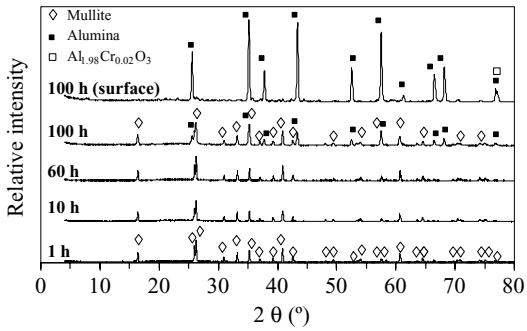

Fig. 3. XRD patterns of powdered and solid samples fired at 1650 °C for different dwell times (10, 20, 40, 60, 80 and 100 h).

of alumina still remains in the sample fired at 1450 °C. For $T > 1450$ °C, mullite is the only crystalline phase detected, the XRD peaks of which always increase with increasing temperature. These differences might be accompanied by a microstructural evolution of the samples. Another determinant factor of the final microstructures is the dwell time. Therefore, the highest temperature (1650 °C) was selected in order to study the microstructural evolution over sintering time, which was varied from 1 to 100 h.

Fig. 2 shows that the visual aspect of the samples practically did not change along the first 60 h of sintering (these entire samples exhibit a beige colour), while significant colour changes occurred for higher sintering times. For 80 h sintering, the sample still shows a central beige coloured region, but the periphery changed to pink, while the entire sample sintered for 100 h exhibits a pink colour. Furthermore, such colour change was accompanied by an increase in surface roughness, also detectable visually, due to well developed crystals.

In order to better understand these microstructural changes, XRD analyses were performed. The results presented in Fig. 3 indicate that mullite is the only crystalline phase present in the samples sintered for times up to 60 h. Some alumina was detected in the sample sintered for 80 h. The amount of alumina re-crystallised from the glassy phase further increased with dwell increasing to 100 h. However, its distribution in the whole sample is not homogeneous as can be concluded from the comparison of the XRD spectra of the powdered sample and of the external surface of the same sample. This last spectrum shows that the surface of the sample is practically composed of alumina and Cr-doped alumina ($Al_{1.98}Cr_{0.02}O_3$). Chromium comes from the Al-rich sludge and is responsible for the pink colour of the Cr-doped alumina crystals.

The SEM micrographs of chemically etched fracture surfaces of the samples sintered for shorter times (10 and 40 h) are shown in Fig. 4a and b, respectively. They confirm that the microstructure of these samples consists of a network of mullite crystals embedded into a glassy phase. The coarsening of the mullite needles with sintering time is the only detectable difference. However, completely different microstructures could be detected for the samples with longer sintering times. Fig. 5a and b refer to samples sintered for 80 h, while Fig. 5c refers to a sample sintered for 100 h. Fig. 5a shows how the enrichment of the sample surface in alumina is accompanied by the increase of surface roughness and porosity. Fig. 5b shows a large alumina crystal near the surface, and an inner region rich in mullite crystals (≈60%) embedded in ≈40% glassy phase. In between there is an intermediate region where the concentration of mullite is significantly lower (≈28%) embedded in an abundant (≈72%) glassy phase. Fig. 5c gives an overview of the microstructure obtained after 100 h sintering, in which the mullite rich regions are confined to small domains located in the inner part of the sample. Large pores can be seen adjacent to α-alumina crystals. These pores arisen from volume changes due to the transformation of a relatively lower dense mullite into a denser α-alumina.

The stereological data gathered from several SEM micrographs are reported in Table 1. From these results, it can be concluded that there is a decrease of the amount of mullite and a concomitant increase of the amount of glassy phase as the dwell time increases. Accordingly, the ratio of

Fig. 2. Cylindrical samples fired at 1650 °C for different dwell times (10, 20, 40, 60, 80 and 100 h).

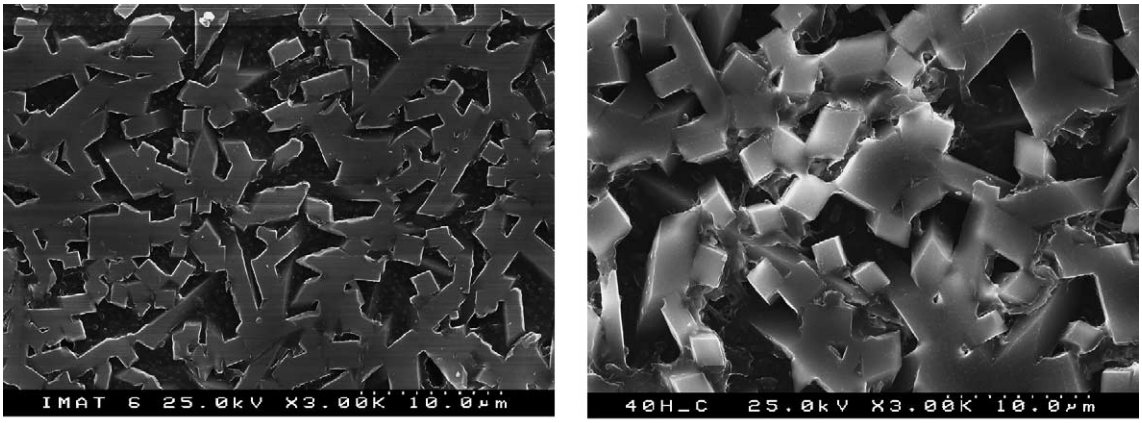

(a) (b)

Fig. 4. SEM microstructures of bodies sintered at 1650 °C for 10 h (a) and 40 h (b).

mullite/glassy phase decreases. As expected, the average grain size also increases with the elapsed time at 1650 °C. These results indicate that the smaller mullite crystals will tend to continuously dissolve into the glassy phase and then will re-precipitate in order to feed the coarser ones, according to the Oswald ripening effect.[25] This can be clearly seen by comparing the Fig. 4a (finer mullite needles) and b (coarser mullite crystals). However, the dissolution seems to be fast when passing from 1 to 10 h sintering at 1650 °C and then continues to progress more slowly, being almost complete at the end of 80 h.

Since the total amount of mullite decreases with sintering time increasing, the excess alumina derived from mullite dissolution would remain either in the glassy phase or be used to nucleate the alumina crystals detected in the samples with longer sintering times. However, the results of EDS analyses made on the glassy phase in the middle of the sample (Fig. 6 and Table 2) show a continuous decrease of the Al_2O_3 content (≈15.4%) along the whole sintering time scale, while crystalline alumina was only detected after 80 h sintering (Fig. 3). This discrepancy might be due to the fact that alumina starts to form at the periphery of the sample, while the EDS analysis was made in the middle of the same. The apparent preferential migration of alumina species to the surface of the sample where the alumina crystals fairly grow needs to be further explained.

Table 2
Chemical compositions of glassy phase of samples fired at 1650 °C during different dwell times

	1 h	10 h	20 h	40 h	60 h	80 h	100 h
Fe_2O_3	1.3	1.62	3.15	2.15	2.08	1.29	1.45
Na_2O	0.75	1.07	2.33	2.59	3.1	4.64	4.37
Al_2O_3	41.61	39.48	34.6	31.55	31.8	29.95	26.2
SiO_2	53.6	54.9	54.16	58.27	58	58.61	62.94
K_2O	0.95	0.9	2.01	1.92	1.92	2.11	1.92
CaO	0.8	0.96	1.7	1.62	1.43	1.47	1.3
MgO	1	1.07	1.1	1.13	0.94	1.21	1.23
TiO_2	–	–	0.95	0.77	0.72	0.72	0.77

Fig. 6 and Table 2 also show that the content of silica in the glassy phase (middle of the sample) steadily increases (≈9.3%) along the whole sintering time scale, accompanied by an increase (≈3.9%) of the Na_2O content. The content of the glassy phase (middle of the sample) in other oxides (MgO, K_2O, TiO_2 and CaO) is almost unaffected after 20 h of sintering.

The re-crystallisation process of alumina seems to be described by the following equation:

$$3Al_2O_3 \cdot 2SiO_2\ (\text{mullite}) \rightarrow 3Al_2O_3\ (\text{alumina}) + 2SiO_2\ (\text{amorphous}) \quad (\text{at } 1650\,^{\circ}\text{C, after } 80\,\text{h sintering})$$

Table 1
Microstructural relevant parameters of samples fired at 1650 °C during different dwell times

Sintering dwell time at 1650 °C (h)	Mullite (M) (%)	Glassy phase (GP) (%)	M/GP ratio	Average grain size (µm)[a]
1	78.1	21.9	3.56	1.75 (± 0.65)
10	68.4	31.6	2.16	2.22 (± 0.53)
20	66.7	33.3	2.00	2.64 (± 0.74)
40	64.4	35.6	1.81	3.56 (± 1.29)
60	62.7	37.3	1.68	4.51 (± 2.40)
80	60.5	39.5	1.53	5.43 (± 1.45)
100	60.2	39.8	1.51	6.33 (± 1.79)

[a] The values in parenthesis correspond to the standard deviation.

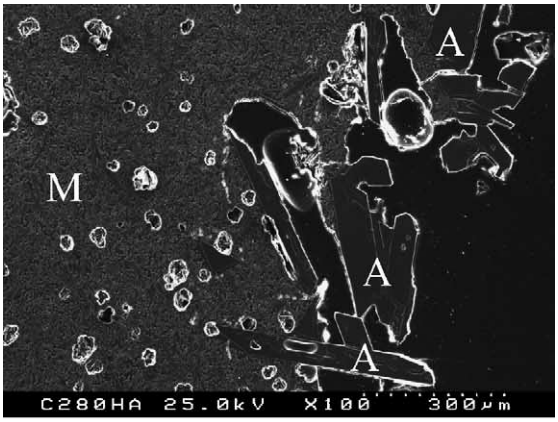

(a)

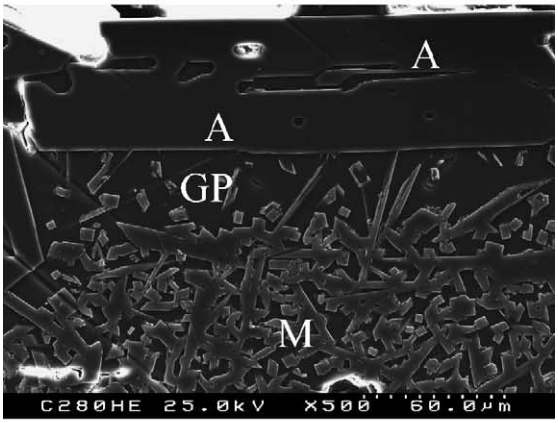

(b)

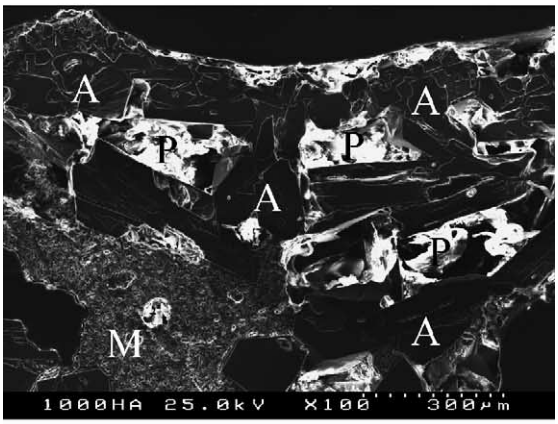

(c)

Fig. 5. SEM microstructures of bodies sintered at 1650 °C for 80 h (a and b) and 100 h (c). A, M, P and GP stand, respectively, for α-alumina, mullite, pores and glassy phase.

In order to better understand the re-crystallisation process of alumina, stereological data was gathered from SEM micrographs of samples sintered for 80 h. The results presented in Table 3 show that the average size of alumina grains, located at, or near the samples' surface, is about 10-times greater in comparison with that of mullite grains located in the inner part of the samples. This explains why the surface

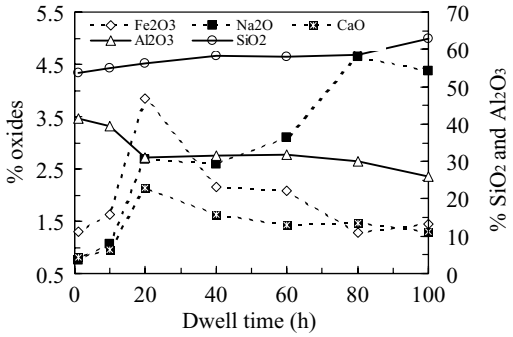

Fig. 6. Evolution of the chemical composition of vitreous phase with dwell time, for samples sintered at 1650 °C. The results are given as percent of different oxides as analysed by EDS.

roughness, as well as the porosity among the alumina grains increase, as shown in Fig. 5a. Table 3 also confirms the abundance (≈72%) of glassy phase near the alumina grains (GP zone in Fig. 5b) when compared with that in the inner mullite rich zone (≈40%).

The results of EDS analyses made to the glassy phase in different regions of the sample sintered for 100 h are plotted in Fig. 7. These results clearly show that the contents of SiO_2 and Na_2O are higher, and that of alumina is lower, near the alumina grains in comparison with the inner mullite rich zone. This suggests that the reactivity of the glassy phase would be higher near the alumina grains, while its viscosity should be lower in comparison with the glass embedding the mullite rich zone.[26]

However, why this re-crystallisation process of alumina occurs preferentially at the surface of the samples is still an open question. It seems reasonable to assume that the most volatile components (alkaline oxides) of the glassy phase will tend to evaporate from the surface of the samples, therefore, originating a concentration gradient that might be favourable to the nucleation of alumina in this region. Some other authors[2,27] refer to the occurrence of silica evaporation and the concomitant increase of relative amount of alumina that might start to crystallise on the surface of mullite grains. After the occurrence of the nucleation events, the alumina

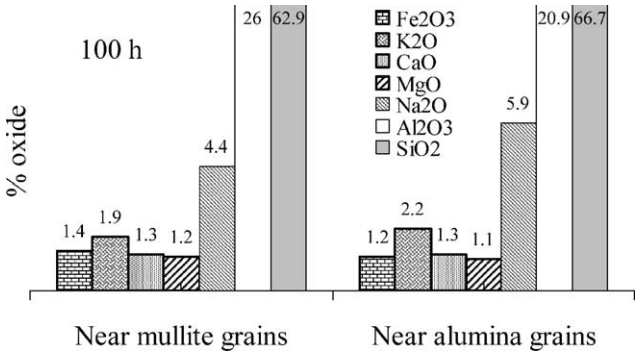

Fig. 7. Chemical compositions of vitreous phase near the mullite and alumina grains for the sample sintered at 1650 °C for 100 h. The results are given as percent of different oxides as analysed by EDS.

Table 3
Microstructural relevant parameters measured in different zones of the samples fired at 1650 °C for 80 h

Zone	Mullite (M) (%)	Alumina (A) (%)	Glassy phase (GP) (%)	(M or A)/GP ratio	Average grain size (μm)[a]
Near the Al_2O_3 grains	27.7	–	72.3	0.38	4.74 (± 1.45)
Near the mullite grains	60.5	–	39.5	1.53	5.43 (± 1.45)
In Al_2O_3 grains	–	71.1	28.9	2.46	96.9 (± 14.65)

[a] The values in parenthesis correspond to the standard deviation.

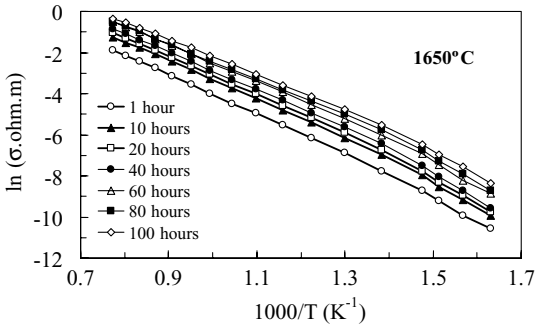

Fig. 8. Arrhenius plot for ceramic samples sintered at 1650 °C during different dwell times.

species will tend to migrate to this region to feed the forming α-alumina crystals. The increasing number of alumina crystals formed at the surface of the sample will act as a barrier that will tend to oppose to the further evaporation process of the most volatile components that will concentrate near the alumina grains. The expected decrease of viscosity of the glassy phase in this region[26] will enhance the diffusion of alumina species from the inner region to the outer region. This interpretation is consistent with the faster development of alumina crystals observed after 80 h of sintering.

The transformation of mullite into alumina and glassy phase is apparently intriguing, since in the silica–alumina system, mullite formation is thermodynamically favoured. From the JANAF Thermochemical Tables,[18] the Gibbs energy variation for the mullite formation at, for example, 1227 °C is $\Delta G = -4899\,\mathrm{kJ\,mol^{-1}}$ compared with that for alumina ($\Delta G = -1196\,\mathrm{kJ\,mol^{-1}}$). This explains why mullite is readily formed even at lower temperatures (<1200 °C). According to Chiang et al.[28] for the same silica–alumina ratio used in our samples, the silica–alumina phase diagram predicts the possibility of precipitation of alumina from the glassy phase at about 1828 °C. Obviously, the presence of other oxides (alkaline, alkaline-hearth, etc.) in our composition will displace the equilibrium conditions to lower temperatures. In fact, Baudín and Villar[15] already reported mullite dissolution at temperatures as low as 1620 °C in the presence of alkalis, even for short dwell times.

Fig. 8 presents the Arrhenius plots of the impedance spectroscopy measurements, which was used to gather complementary data to better understand the microstructutal analyses. The most salient features of the electrical behaviour curves are as follows:

1. The electrical conductivity gradually increases with increasing the sintering time. This might be explained by the progressive dissolution of the most resistive mullite phase and the concomitant increasing amount of glassy phase, which is predictably more conductive. It is worth-

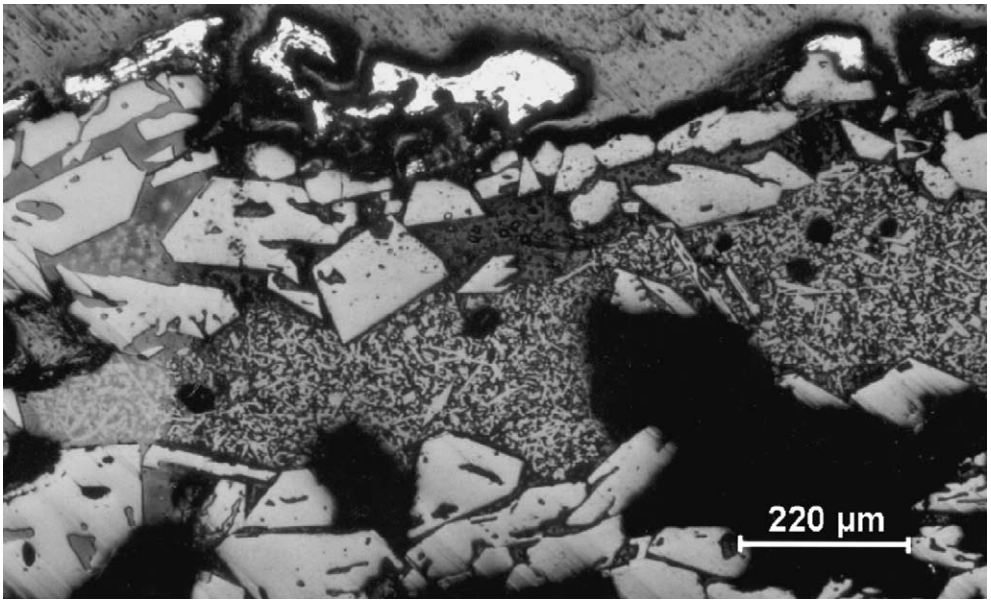

Fig. 9. Optical microscopy view of sample sintered at 1650 °C for 100 h, showing a mullite central region of about 200 μm.

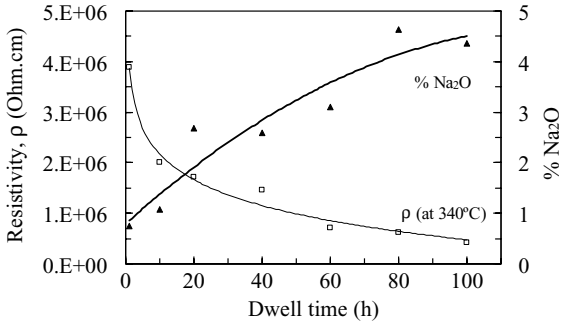

Fig. 10. Evolution of electrical resistivity measured at 340 °C and the amount of Na_2O in the glassy phase, as a function of dwell time.

while to note that the more drastic change in terms of electrical conductivity occurred within the time interval between 1 and 10 h, therefore, confirming the stereological data gathered from the SEM microstructures.

2. The curves corresponding to 60 and 80 h are very close to each other indicating that the system is approaching an equilibrium situation in terms of the relevance of the different factors that account for the electrical behaviour.
3. After 80 h sintering the electrical conductivity stills increase, despite the strong formation of alumina crystals near the surface, which are very resistive. However, those grains are not completely connected to form an insulating barrier and the progressive increase of glassy phase, predictably less viscous (enriched in alkalis, especially sodium oxide), enhances the number of easy pathways for the ionic transport. At the same time the thickness of insulated mullite central region progressively diminishes for longer dwell time. Fig. 5a and b clearly show that after 80 h this layer still corresponds to the total sample thickness while sample exposed for 100 h shows an average thickness of about 200 μm (Fig. 9). Fig. 10 confirms the close relationship between the electrical resistivity of the sample and the Na_2O content in the glassy phase.

The comparison of the results obtained by impedance spectroscopy with the EDS analysis and stereological data enable to conclude that there is a good consistency, and that impedance spectroscopy is a good complementary technique to access the microstructural development during sintering of the samples used in the present work.

4. Conclusions

Mullite-based refractory ceramics could be produced from an industrial Al-rich sludge and other low cost natural raw materials. However, the impurities incorporated with the batch components prevent their use at very high temperatures. The main structural changes that might occur at 1650 °C are as follows: (i) a preferential dissolution of the smaller mullite grains in the glassy phase and its partial re-precipitation onto the coarser ones, according to the Ostwald ripening effect, for dwell times <80 h; (ii) the development of large α-alumina and Cr-doped alumina grains at the surface of the specimens, accompanied by pores' formation in the vicinity of alumina grains, an overall increase of surface roughness for dwell times >80 h; and (iii), a concomitant generation of concentration gradients within the glassy phase, enriched in alkalines and almost depleted in Al near alumina grains. The dissolution of mullite and the enrichment of the matrix glassy phase in alkaline species enhanced the electrical conductivity of the material, enabling a close relationship to be observed between the microstructural changes accessed by various characterisation techniques and by impedance spectroscopy.

Acknowledgements

The authors are grateful to Foundation for Science and Technology of Portugal and to Prodep III (medida 5/5.3) for the financial support.

References

1. Shin, H., Kim, C.-S. and Chang, S.-N., Mullitisation from a multicomponent oxide system in the temperature range 1200–1500 °C. *J. Am. Ceram. Soc.* 2000, **83**(5), 1237–1240.
2. Souto, A., Guitian, F. and Aza, S., Purification of mullite by reduction and volatilization of impurities. *J. Am. Ceram. Soc.* 1999, **82**(10), 2660–2664.
3. Camerucci, M. A., Urretavizcaya, G., Castro, M. S. and Cavalieri, A. L., Electrical properties and thermal expansion of cordierite and cordierite–mullite materials. *J. Eur. Ceram. Soc.* 2001, **21**, 2917–2923.
4. Kleebe, H.-J., Siegelin, F., Straubinger, T. and Ziegler, G., Conversion of Al_2O_3–SiO_2 powder mixtures to 3:2 mullite following the stable or metastable phase diagram. *J. Eur. Ceram. Soc.* 2001, **21**, 2521–2533.
5. Redfern, S. A. T., The kinetics of dehydroxylation of kaolinite. *Clay Miner.* 1987, **22**, 447–456.
6. Chaudhuri, S. P., Mullite in hard porcelain. *Trans. Indian Ceram. Soc.* 1973, **32**(6), 135–139 (Reprint).
7. Chen, C. Y. and Tuan, W. H., The processing of kaolin powder compact. *Ceram. Int.* 2001, **27**, 795–800.
8. Lee, W. E. and Iqbal, Y., Influence of mixing on mullite formation in porcelain. *J. Eur. Ceram. Soc.* 2001, **21**, 2583–2586.
9. Chen, C. Y., Lan, C. S. and Tuan, W. H., Microstructural evolution of mullite during the sintering of kaolin powder compacts. *Ceram. Int.* 2000, **26**, 715–720.
10. McConville, C. J., Lee, W. E. and Sharp, J. H., Microstructural evolution in fired kaolinite. *Br. Ceram. Trans.* 1998, **97**(4), 162–168.
11. Iqbal, Y. and Lee, W. E., Fired porcelain microstructures revisited. *J. Am. Ceram. Soc.* 1999, **82**(12), 3584–3590.
12. Iqbal, Y. and Lee, W. E., Microstructural evolution in triaxial porcelain. *J. Am. Ceram. Soc.* 2000, **83**(12), 3121–3127.
13. Olhero, S. M., Tarì, G. and Ferreira, J. M. F., Feedstock formulations for direct consolidation of porcelains with polysaccharides. *J. Am. Ceram. Soc.* 2001, **84**(4), 719–725.
14. Lucas, D. B., *Development of Ceramic Bodies Maturing at Low Temperatures*. Master Science dissertation, North Staffordshire Polytechnic, Stoke-on-Trent, 1977.
15. Baudín, C. and Villar, M. P., Influence of thermal aging on microstructural development of mullite containing alkalis. *J. Am. Ceram. Soc.* 1998, **81**(10), 2741–2745.

16. Sacks, M. D., Wang, K., Scheiffele, G. W. and Bozkurt, N., Effect of composition on mullitisation behavior of α-alumina/silica microcomposite powders. *J. Am. Ceram. Soc.* 1997, **80**(31), 663–672.
17. *Mullite and Mullite Ceramics*, ed. H. Schneider, K. Okada and J. Pask. John Wiley & Sons Ltd, Chichester, 1994.
18. JANAF Thermochemical Tables, Ref. Data 14. *J. Phys. Chem.* 1985, 156.
19. Ribeiro, M. J., Tulyaganov, D. U., Ferreira, J. M. and Labrincha, J. A., Recycling of Al-rich industrial sludge in refractory ceramic pressed bodies. *Ceram. Int.* 2002, **28**, 319–326.
20. Tulyaganov, D. U., Olhero, S. M. H., Ribeiro, M. J., Ferreira, J. M. and Labrincha, J. A., Mullite–alumina refractory ceramics obtained from mixtures of natural common materials and recycled Al-rich anodising sludge. *J. Mater. Synth. Proc.* 2002, **10**(6), 311–318.
21. Pereira, D. A., Couto, D. M. and Labrincha, J. A., Incorporation of aluminum-rich residues in refractory bricks. *Ceram. Forum Int.* 2000, **77**(7), 21–25.
22. Pereira, F. R., Hotza, D., Segadães, A. M. and Labrincha, J. A., Recycling of several wastes as refractory materials. In *Proceedings of UNITECR'03*. TARJ, Osaka, Japan, 2003, pp. 150–153.
23. Underwood, E. E., *Quantitative Stereology*. Addison-Wesley, Georgia, 1970.
24. Abrantes, J. C. C., Labrincha, J. A. and Frade, J. R., Representations of impedance spectra of ceramics: Part I. Simulated study cases. *Mat. Res. Bull* 2000, **35**(6), 955–964.
25. Ardell, A. J., The effect of volume fraction on particle coarsening: theoretical considerations. *Acta Metal.* 1972, **20**, 61–71.
26. Navarro, J. M. F., *El Vidrio* (*2nd ed.*). Consejo Superior de Investigaciones Científicas, Fundación Centro Nacional del Vidrio, Madrid, 1991, pp. 344–345.
27. Solid solutions in the system Al_2O_3–SiO_2. In *Chemistry of Silicates and Oxides*, ed. N. A. Toropov and F. Y. Galakhov. Nauka, Leningrad, 1974, pp. 198–202 (in Russian).
28. Chiang, Y. -M., Birnie III, D. P. and Kingery, W. D., *Physical Ceramics, Principles for Ceramic Science and Engineering*. John and Wiley & Sons, Inc., Tucson, AZ, 1997.